JOURNAL OF CATALYSIS 139, 1–18 (1993)

Interactions in Alumina-Based Iron Oxide–Vanadium Oxide Catalysts under High Temperature Calcination and SO_2 Oxidation Conditions

F. T. CLARK,*,[1] M. C. SPRINGMAN,* D. WILLCOX,† AND I. E. WACHS‡

*Amoco Oil Research Department, Naperville, Illinois 60566; †University of Illinois–Chicago, Chicago, Illinois 60607; and ‡Zettlemoyer Center for Surface Studies, and Department of Chemical Engineering, Lehigh University, Bethlehem, Pennsylvania 18015

Received March 30, 1992; revised August 4, 1992

Depending on such variables as vanadium oxide content, calcination temperature and the content of sulfur dioxide in the oxidizing atmosphere, wide variations in surface area, phase composition, metal oxide–support interactions, and inter- and intraparticle metal oxide migration were observed in γ-alumina (PHF) catalysts containing iron oxide and vanadium oxide—two common contaminant metal oxides found in refinery catalysts—under conditions simulating FCC or resid hydrotreating catalyst regeneration. Samples were subjected to a wide range of calcination temperatures and were tested for the catalytic oxidation of sulfur dioxide by thermal gravimetric analysis (TGA). Catalysts were characterized by a number of techniques, including porosimetry, X-ray photoelectron spectroscopy (XPS), X-ray diffraction (XRD), and Mössbauer and ^{51}V-NMR spectroscopy. TGA tests indicated that both iron and vanadium oxides catalyzed the formation of aluminum sulfate at lower temperatures compared with blank alumina, but that iron–vanadium mixed oxides were inactive. The results of this study suggest a possible need to incorproate sulfur dioxide in typical fluid catalytic cracking (FCC) laboratory steaming experiments, especially if contaminant metal oxides have been artificially introduced. Such incorporation may induce different metal oxide–metal oxide interactions and alumina phase transitions compared with steamings in the absence of sulfur dioxide and may better test the true passivating potential of commercially available SO_x additives.

INTRODUCTION

Iron and vanadium are among the major contaminants found in typical petroleum-based refinery catalysts (*1*, *2*). The influence of oxidative treatments on vanadium migration and subsequent FCC catalyst activity have been extensively studied (*2–8*). Vanadium pentoxide is generally immiscible with alumina and certain metal oxides under oxidizing conditions (*9–11*). Group VIII metals, however, are generally miscible with alumina and may easily form low-surface-area spinels at high temperatures (*12–19*). Little is known about the interaction of a miscible oxide, like iron, with an immiscible oxide, like vanadium, on the same catalyst particle following high-temperature calcinations. In addition, the influence of sulfur dioxide, a by-product of regeneration processes, on the iron–vanadium interaction is not understood.

FCC catalyst regeneration, FCC SO_x removal, and resid hydrotreating catalyst regeneration are three areas for which studies of iron–vanadium–support interactions are desirable. Vanadium poisons FCC catalyst activity, iron alters FCC catalyst selectivity, and both promote the oxidative adsorption of sulfur dioxide in the FCC catalyst matrix

[1] To whom correspondence should be addressed at: Mail Station H-4, Amoco Oil Company, Amoco Research Center, P.O. Box 3011, Naperville, IL 60566.

0021-9517/93 $5.00

(*2*, *13*, *20*, *21*). In addition, previous studies of regenerated reside hydrotreating catalyst showed that undesirable catalyst softening and mesopore sintering correlate with the formation of mixed iron–vanadium oxides following high-temperature oxidations in the presence of sulfur dioxide (*22*).

The purpose of this paper is to study the interactions of iron and vanadium oxides on an alumina support subjected to high-temperature calcination treatments. In addition, the accumulation of aluminum sulfate, which forms by the reaction of alumina with sulfur trioxide, was monitored by thermal gravimetric analysis (TGA) of the samples exposed to sulfur dioxide. Following these treatments, selected catalysts were analyzed by a number of techniques, including XPS, ICP, XRD, porosimetry, Mössbauer spectroscopy, and ^{51}V-MAS-NMR.

METHODS

Catalysts

The starting support for all catalysts was PHF gamma-alumina extrudates (196 m^2/g). PHF is the American Cyanamid tradename for highly pure gamma-alumina, which contains only trace (ppm) quantities of sulfate or contaminant metals such as Na or Fe. The extrudates were crushed to a fine powder (360 mesh) and dried at 540°C for 90 min prior to impregnation and calcination. Catalysts were prepared by the incipient wetness impregnation technique. Vanadium-based catalysts were prepared by dissolving vanadium triisopropoxide oxide (Alfa, 95–99%) in isopropanol (Mallinckrodt, 0.028% H_2O). Vanadium tri-isopropoxide oxide was chosen as the vanadium precursor because its solubility was high in alcohol and its use allowed 5-wt% V_2O_5 levels to be attained after a single impregnation. Due to the water-sensitive nature of the vanadium precursor, all impregnations were performed in a nitrogen-purged glove box. Iron-based catalysts were prepared by dissolving iron nitrate nano-hydrate (EM Science) in methanol (Aldrich, .04% H_2O). After impregnations were performed, samples were dried overnight at 100°C in flowing nitrogen using a small fixed-bed quartz tube. The iron–vanadium catalysts were prepared by first impregnating with vanadium, then drying at 100°C in nitrogen, then impregnating with iron and drying at 100°C in nitrogen. Separate impregnations were required because the iron and vanadium salts were not soluble in the same alcohol. Vanadium was impregnated first to ensure uniform coverage. Iron nitrate was chosen as the precursor metal salt because of its high solubility in methanol. Exposure of the water-sensitive vanadium-impregnated support to a methanol solution was deemed a less harmful way to incorporate iron compared with an aqueous impregnation. Catalysts were calcined for 2 hr in dry flowing air at temperatures ranging from 500 to 900°C.

The surface coverage of V_2O_5 on the alumina support after calcination at 500°C was about 25% monolayer for a 5-wt% V_2O_5 loading and about 50% monolayer for a 10-wt% V_2O_5 loading, based on Raman analyses of these (43) and other related samples (*29*, *34*). A 5-wt% V_2O_5 and/or a 5-wt% Fe_2O_3 metal loading on the support was chosen to simulate metal-contaminated regenerated resid hydrotreating catalysts found in a typical refinery.

An iron–vanadium oxide standard, $FeVO_4$, was prepared according to the method of Wong-Ng *et al.* (*23*), followed by repeated washing in dilute (0.1 *M*) nitric acid at 50°C to remove residual vanadium pentoxide. XRD analysis indicated high crystallinity of $FeVO_4$ with no traces of V_2O_5. A standard of aluminum vanadate, $AlVO_4$, was supplied by Exxon.

Table 1 lists the catalysts, calcination temperatures and analyses discussed in this paper.

Catalyst Characterization

XPS spectra were recorded on a Surface Science Instrument SSX-100 spectrometer using monochromatic Al$K\alpha$ radiation ($h\nu$ = 1486.6 eV) at a take-off angle of 35°. A typical sampling size for XPS analysis was 600

TABLE 1

Catalysts, Calcination Treatments, and Analyses

Catalyst[a]	Calcination temp. (°C)	Analyses						
5% V_2O_5	500	V-NMR	TGA	BET	XPS	ICP	XRD[c]	
	700	V-NMR		BET	XPS		XRD	
	800				XPS		XRD	
	900	V-NMR		BET	XPS	ICP	XRD	
10% V_2O_5	500		TGA				XRD[b]	
5% Fe_2O_3	500		TGA	BET	XPS	ICP	XRD[c]	MOSS
	700			BET	XPS	ICP	XRD	
	800				XPS		XRD	
	900			BET	XPS	ICP	XRD	MOSS
10% Fe_2O_3	500		TGA				XRD[b]	
5% Fe_2O_3/5% V_2O_5	500	V-NMR	TGA	BET	XPS	ICP	XRD[c]	MOSS
	700	V-NMR		BET	XPS		XRD	
	800				XPS			
	900	V-NMR		BET	XPS	ICP	XRD	MOSS
5% Fe_2O_3 + 5% V_2O_5	500		TGA		XPS			
(physical mixture)	900	V-NMR		BET				
Blank PHF alumina	500		TGA	BET			XRD[c]	
	700			BET				
	900			BET				
$AlVO_4$ Standard	840	V-NMR					XRD	
$FeVO_4$ Standard	840	V-NMR					XRD	MOSS
Blank PHF + $FeVO_4$ mixture	—		TGA					

[a] All catalysts were supported on PHF γ-alumina powder.
[b] XRD on TGA postmortem residue only.
[c] XRD on air-calcined sample and TGA postmortem residue.

μm at an analyzer pass energy of 100 eV. Binding energies were referenced to aluminum 2*p* (74.5 eV).

Elemental analyses were performed on an Applied Research Model 3560 ICP Atomic Emission Analyzer with a precision of ±5%. Samples were prepared by standard acid digestion. Surface area and porosity measurements were determined by nitrogen desorption isotherms using the BJH method (*44*) on a Micromeretics 2400 instruments. X-ray diffraction patterns were recorded at standard conditions on a Scintag PAD V Diffractometer equipped with an Ortec intrinsic germanium solid state detector. The X-ray source was unfiltered Cu$K\alpha$ radiation with a beam intensity of 1.8 kW. Phase identification was performed using the Powder Diffraction File.

^{57}Fe Mössbauer spectra of the samples were obtained through Dr. William Reiff of Mössbauer Spectroscopy Consultants in Bethlehem, Massachusetts. The catalysts were analyzed with a conventional constant-acceleration spectrometer operated in the time mode using 100-mCi 57-Co/Rh matrix as the gamma-ray source. Iron foil was the reference. Least-squares Lorentzian fits of the Mössbauer spectra were accomplished using a previous method (*24*). Vanadium-51-NMR spectra were obtained using a rotation synchronized spin echo technique with magic-angle spinning (MAS) at a rate of 5.5 kHz on a Varian CMX-200 spectrometer. The resonance frequency for vanadium-51 was 52.6 MHz. The magnetic field was 4.7 Tesla. All chemical shifts were referenced against liquid $VOCl_3$ with use of a spinning sample of solid sodium vanadate ($NaVO_3$) as a secondary reference material. In some

^{51}V-MAS-NMR spectra of alumina-supported vanadium samples, a spurious peak at about −40 ppm is observed due to an artifact known as aluminum "aliasing." Aliasing sometimes occurs when two nuclei have similar resonance frequencies (in our case, aluminum (52.1 MHz) and vanadium (52.6 MHz). Aliasing is usually minimized by the appropriate choice of cutoff filters and should be considered a minor instrument artifact that does not influence the information content of the ^{51}V-MAS-NMR spectra shown in this paper.

Thermal Gravimetric Analysis—SO_2 Oxidation

TGA analyses were performed on a DuPont 951 Thermogravimetric Analyzer coupled with a DuPont 9900 Processor. The source of the SO_2 gas was Matheson, available as a mixture of 10% SO_2, 10% O_2, and argon balance. Dilution of the TGA analyses were performed on a DuPont 951 Thermogravimetric Analyzer coupled with a DuPont 9900 Processor. The source of the SO_2 gas was Matheson, available as a mixture of 10% SO_2, 10% O_2, and argon balance. Dilution of the SO_2 gas with argon prior to contact with the sample was used to obtain the desired dosing concentration: 5% SO_2, 5% O_2, with argon gas as the balance. This concentration was chosen to simulate the expected partial pressures of sulfur dioxide and oxygen under commercial resid hydrotreating catalyst regeneration conditions.

TABLE 2

Programmed Catalyst Treatment for SO_2 Oxidation by Thermal Gravimetric Analysis

- Sample size 20 mg.
- Pre-dry 700°C, 30 min in argon; cool to 200°C in argon.
- Ramp from 200 to 900°C (10°C/min) in 5% SO_2 + 5% O_2 + argon.
- Hold at 900°C for 1 hr in 5% SO_2 + 5% O_2 + argon.
- Cool from 900 to 200°C in argon.
- Resulfate sample: Ramp from 200° to about 600°C (10°C/min) or until sample weight gain is maximized.
- Cool to room temperature in 5% SO_2 + 5% O_2 + argon.

The flow rate of the gas was 100 cc/min. Table 2 summarizes the programmed treatment.

RESULTS

Elemental Analyses/XPS

Table 3 lists the bulk elemental compositions for the 5% V_2O_5, 5% Fe_2O_3, and the 5% V_2O_5–5% Fe_2O_3 catalysts after various calcination temperatures expressed both as atomic metal ratios (V/Al and Fe/Al) as well as atomic ratios normalized to the observed ratio at 500°C. Compositions were determined by ICP. Analogous results are shown in Table 4 for surface concentrations by XPS.

All vanadium in the samples was in the

TABLE 3

Catalyst Bulk Composition by ICP

Catalyst	Calcination temp. (°C)	V (wt%)	Fe (wt%)	Al (wt%)	V/Al	Normalized V/Al	Fe/Al	Normalized Fe/Al
5% V_2O_5	500	2.50	—	49	0.051	1.00	—	—
	900	2.59	—	49	0.052	1.02	—	—
5% Fe_2O_3	500	—	3.30	48	—	—	.068	1.00
	700	—	3.38	50	—	—	.068	1.00
	900	—	3.36	48	—	—	.070	1.03
5% V_2O_5–5% Fe_2O_3	500	2.55	3.25	49	0.052	1.00	.066	1.00
	900	3.25	3.25	48	0.053	1.02	.067	1.02

TABLE 4

Catalyst Surface Composition by XPS

Catalyst	Calcination temp. (°C)	Binding energy (eV)		V (Atom%)	Fe (Atom%)	Al (Atom%)	V/Al	V/Al (Normalized)	Fe/Al	Fe/Al (Normalized)
		Fe ($2p_{3/2}$)	V ($2p_{3/2}$)							
5% V_2O_5	500	—	517.1	1.0	—	35.5	0.028	1.0	—	—
	700	—	517.1	1.1	—	34.4	0.032	1.1	—	—
	800	—	517.3	1.1	—	33.4	0.033	1.2	—	—
	900	—	517.3	3.5	—	31.6	0.111	4.0	—	—
5% Fe_2O_3	500	711.2	—	—	0.4	35.5	—	—	0.011	1.0
	700	711.4	—	—	0.4	36.8	—	—	0.011	1.0
	800	711.3	—	—	0.5	31.8	—	—	0.015	1.4
	900	711.5	—	—	0.6	33.8	—	—	0.017	1.6
5% V_2O_5–5% Fe_2O_3	500	710.8	517.1	0.8	0.4	35.4	0.023	1.0	0.011	1.0
	700	711.5	517.2	1.1	0.4	34.4	0.032	1.4	0.012	1.1
	800	711.1	517.7	1.3	0.4	34.0	0.038	1.7	0.012	1.1
	900	711.1	517.2	3.7	0.5	30.0	0.123	5.4	0.017	1.6

+5 oxidation state as inferred from the vanadium $2p_{3/2}$ binding energy of about 517.1 eV. No V(IV) was detected. All iron in the samples was in the +3 oxidation state as inferred from the iron $2p_{3/2}$ binding energy of about 711.5 eV. Table 4 shows that the surface V/Al ratio increases fourfold from about 0.028 to 0.111 for the 5% V_2O_5 catalyst and over fivefold from 0.023 to 0.123 for the 5% V_2O_5–5% Fe_2O_3 catalyst as calcination temperature increases from 500 to 900°C. However, over this same range of calcination temperatures, bulk V/Al ratios are relatively constant for the two catalysts, as seen in Table 3.

Porosity

Table 5 shows that the 5% V_2O_5 catalyst, the iron–vanadium catalyst, and, to a lesser extent, the physical mixture of 5% V_2O_5 and 5% Fe_2O_3 catalysts lost significantly more surface area compared to the 5% Fe_2O_3 catalyst or the alumina blank after 900°C calcination. Iron, like nickel, has little effect on the macroporosity of the support. The loss in surface area was most pronounced for the 5% Fe_2O_3–5% V_2O_5 catalyst. At temperatures of 700°C or less, all catalysts had roughly the same surface area of about 170–190 m^2/gram and a pore volume of about 0.44–0.51 cc/g. Figure 1 shows that the catalyst pore volume decreased and that the catalyst mesopore diameter increased in the following order:

$$Al_2O_3 \approx 5\%\ Fe_2O_3 < 5\%\ Fe_2O_3 + 5\%\ V_2O_5 \ (\text{Physical mixture}) < 5\%\ V_2O_5 < 5\%\ Fe_2O_3\text{–}5\%\ V_2O_5.$$

X-ray Diffraction

Table 6 lists phases detected by X-ray diffraction in samples following various calcination treatments. At calcination temperatures of 700°C or lower, only γ-alumina was detected in all catalysts. However, at

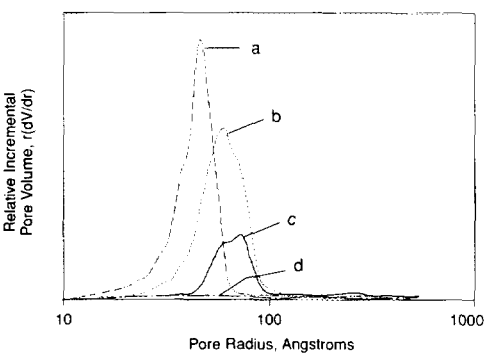

FIG. 1. Pore distribution of catalysts after 900°C calcination: (a) 5% Fe_2O_3 or blank alumina (190 m^2/g), (b) physical mixture 5% Fe_2O_3 + 5% V_2O_5 (122 m^2/g), (c) 5% V_2O_5 (43 m^2/g), and (d) 5% Fe_2O_3–5% V_2O_5 (5 m^2/g).

TABLE 5

Porosity of Catalysts

Catalyst	Calcination temp. (°C)	BET surface area (m^2g)	Surface area retained (%)	Pore volume (N_2 BJH) (cc/g)	Average pore diameter (4V/A)A
5% V_2O_5	500	191	100	0.47	98
	700	189	99	0.47	99
	900	44	23	0.18	164
5% Fe_2O_3	500	184	100	0.45	98
	700	175	95	0.46	105
	900	157	85	0.44	112
5% V_2O_5–5% Fe_2O_3	500	190	100	0.44	93
	700	173	91	0.45	104
	900	6	3	0.02	133
PHF alumina blank	500	191	100	0.51	107
	700	183	96	0.50	109
	900	161	84	0.49	122
5% V_2O_5 + 5% Fe_2O_3 (physical mixture)	900	122	64	0.45	148

900°C, the 5% V_2O_5 catalyst formed θ-alumina and a minor phase of crystalline vanadium pentoxide; the 5% Fe_2O_3 catalyst and the blank alumina remained in the γ-alumina phase; finally, the iron–vanadium catalyst formed a mixture of δ- and κ-alumina phases, as well as a minor phase of crystalline vanadium pentoxide. Supporting XRD diffractograms for these assignments are presented later.

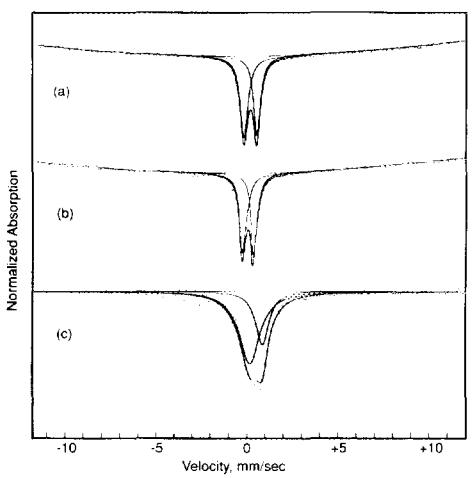

FIG. 2. Normalized Mössbauer spectra of 5% Fe_2O_3–5% V_2O_5 catalyst calcined at 900°C. Spectra obtained at (a) 293 K, (b) 77 K, and (c) 4.2 K.

Mössbauer Spectroscopy

Figure 2 shows normalized Mössbauer spectra obtained at (a) 293, (b) 77, and (c) 4.2 K for the 5% Fe_2O_3–5% V_2O_5 sample calcined at 900°C. Analogously, Figure 3 shows normalized spectra obtained at (a) 293, (b) 77, (c) 4.2, and (d) 1.4 K for the 5% Fe_2O_3 sample calcined at 900°C. For the 500°C samples, only 293-K spectra were obtained and were similar in character to those

TABLE 6

XRD Analyses of Catalysts after Calcination

Catalyst	Calcination temp. (°C)	XRD phases
5% V_2O_5	500, 700, 800	γ-Alumina (Major)
	900	θ-Alumina (Major)
		V_2O_5 (Minor)
5% Fe_2O_3	500, 700, 900	γ-Alumina (Major)
5% V_2O_5–5% Fe_2O_3	500, 700, 800	γ-Alumina (Major)
	900	δ-Alumina (Minor)
		K-Alumina (Major)
		V_2O_5 (Minor)
PHF alumina blank	500, 700, 900	γ-Alumina (Major)

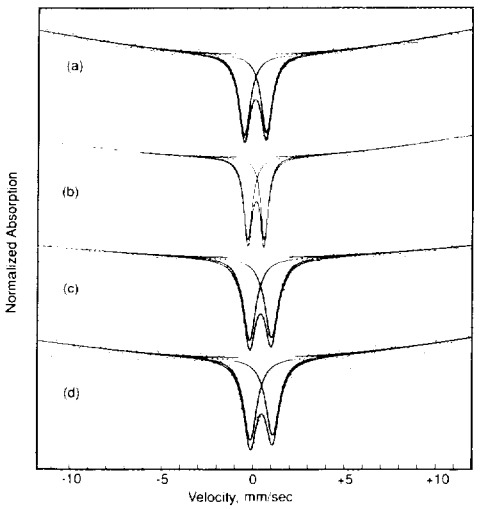

FIG. 3. Normalized Mössbauer spectra of 5% Fe_2O_3 catalyst calcined at 900°C. Spectra obtained at (a) 293 K, (b) 77 K, (c) 4.2 K, and (d) 1.4 K.

shown in Figs. 2 and 3. All spectra shown in these figures contain a superparamagnetic doublet, which has been assigned by others to Fe(+3) ions absorbed into the alumina lattice as a solid solution (*14–19*). Since different sample sizes were used, the spectra in Figs. 2 and 3 are normalized. Normalization has no bearing on determinations of the isomer shift or the quadrupole splittings discussed below.

Table 7 shows room-temperature isomer shifts of 0.33 and 0.22 mm/sec for the 5% Fe_2O_3 catalyst after 500 and 900°C calcinations, respectively, which do not differ significantly within the moderate experimental uncertainty of ±0.07 mm/sec. The respective isomer shifts for the 5% Fe_2O_3–5% V_2O_5 catalyst are 0.59 and 0.57 mm/sec after 500 and 900°C calcinations. These isomer shifts indicate the presence of ferric iron in the samples (*14, 25, 26*), in agreement with the XPS results. Within the experimental uncertainty, the isomer shifts of the 900°C sampels in Table 7 obtained at reduced spectrum temperatures are more or less the same for the 5% Fe_2O_3 catalyst but decrease for the 5% Fe_2O_3–5% V_2O_5 catalyst. The Mössbauer spectra unfortunately do not confirm or rule out the presence of tetrahedral iron in the samples due to the experimental scatter (*28*).

Values for the room temperature quadrupole splittings in Table 7 are relatively constant within the experimental uncertainty for the 5% Fe_2O_3 catalyst as the calcination temperature increases from 500 to 900°C. However, for the 5% Fe_2O_3–5% V_2O_5 catalyst, these values decrease markedly from 1.05 to about 0.74 for the 500 to 900°C samples at room temperature.

A room temperature Mössbauer spectrum of the $FeVO_4$ standard was similar to that reported by Robertson (*47*). None of the 5% Fe_2O_3–5% V_2O_5 samples in Table 7 showed evidence of any $FeVO_4$ formation, a result that was also verified in separate Raman analyses (*43*).

^{51}V NMR (*Magic Angle Spinning*)

Figure 4 shows ^{51}V-MAS-NMR spectra of several reference vanadium (+5) compounds, including $AlVO_4$ (a), V_2O_5 (b), and $FeVO_4$ (c). The featureless spectra of $FeVO_4$ (c) reflects the close proximity of iron, a paramagnetic metal, to the vanadium in the compound, which dampens the vanadium signal. Previous work in our laboratory using both XRD and V-NMR analyses

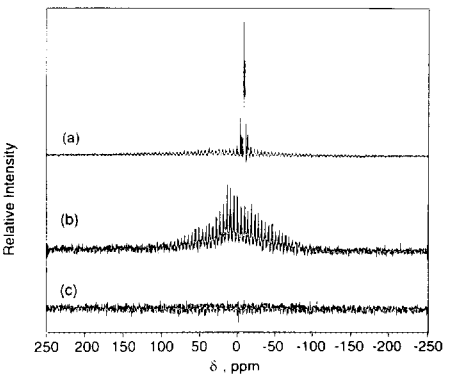

FIG. 4. ^{51}V-MAS-NMR spectra of reference vanadium (+5) compounds: (a) $AlVO_4$, (b) V_2O_5, and (c) $FeVO_4$.

TABLE 7

Mössbauer Results

Catalyst	Calcination temp. (°C)	Spectrum temp. (K)	Isomer shift (mm/sec)[a]	Quadropole splitting (mm/sec)[a]
5% Fe_2O_3	500	293	0.33	0.99
	900	293	0.22	1.21
		77	0.34	0.91
		4.2	0.34	1.12
		1.4	0.39	1.14
5% Fe_2O_3–5% V_2O_5	500	293	0.59	1.05
	900	293	0.57	0.74
		77	0.28	0.60
		4.2	0.43	0.65

[a] Uncertainty is ±0.07 mm/sec, relative to iron foil.

of selected samples has shown that distances (V_2O_5 crystallite sizes) of less than approximately 50 Å cause sufficient signal dampening to occur (*37*).

Figure 5 shows ^{51}V-MAS-NMR spectra of 5% V_2O_5 catalysts after calcination at 500 (a), 700 (b), and 900°C (c), as well as the spectra of reference vanadium pentoxide (d). Except for a sharp band at about 40 ppm due to an instrument artifact (alumina aliasing), the spectra at 500 (a) and 700°C (b) were identical. The broad "hump" at about 0 ppm indicated a well-dispersed surface vanadate phase. Indeed, separate Raman analyses (*43*) detected a broad band at about 930–940 cm^{-1} for the 500 and 700°C samples of 5% V_2O_5, indicating a well-dispersed, tetrahedrally coordinated metavanadate species (VO_4), as confirmed in other studies (*9*, *29–32*). The spectrum of the 5% V_2O_5 sample after 900°C calcination (c) is similar to reference V_2O_5 (d), except for a feature at about −200 ppm, the origin of which is discussed below. Under static NMR conditions, a similar sample gave an NMR spectrum similar to that reported in the literature (*33*, *34*).

Figure 6 shows ^{51}V-MAS-NMR spectra of the 5% Fe_2O_3–5% V_2O_5 sample after calcination at 500 (a), 700 (b), and 900°C (c), as well as the spectra for reference vanadium pentoxide (d). The spectra of the samples calcined at 500 (a) and 700°C (b) are featureless, apparently due to the close proximity of iron to vanadium on the surface. However, the spectrum of the 900°C sample (c) contains substantial contributions from crystalline vanadium pentoxide on the catalyst surface, with a spectrum similar to that of the reference (d). Significantly, separate Raman analyses (*43*) detected no iron–vanadium mixed oxide formation, such as $FeVO_4$. Also of note, the feature at about −200 ppm was not detected in Fig. 6c for the 5% V_2O_5–5% Fe_2O_3 sample, unlike Fig. 5c for the 5% V_2O_5 sample. The −200 ppm

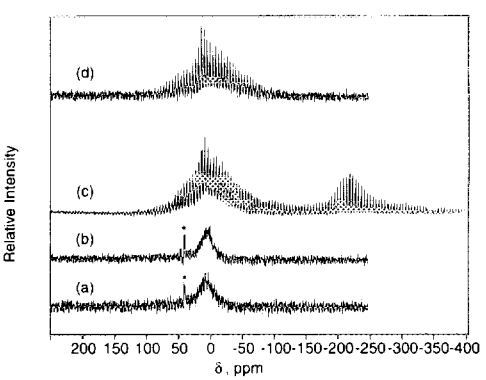

FIG. 5. Effect of calcination temperature on ^{51}V-MAS-NMR spectra of 5% V_2O_5 catalyst: (a) 500°C, (b) 700°C, (c) 900°C, (d) reference V_2O_5, and (*) "alumina aliasing"—instrument artifact.

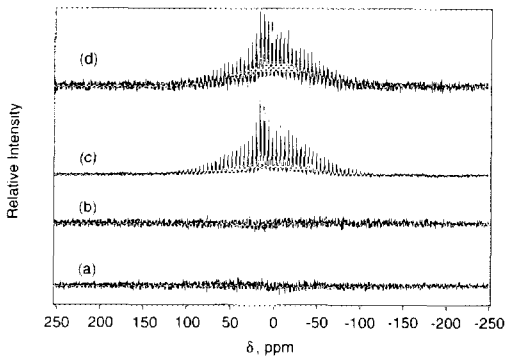

FIG. 6. Effect of calcination temperature on ^{51}V-MAS-NMR spectra of 5% Fe_2O_3–5% V_2O_5 catalyst: (a) 500°C, (b) 700°C, (c) 900°C, and (d) reference V_2O_5.

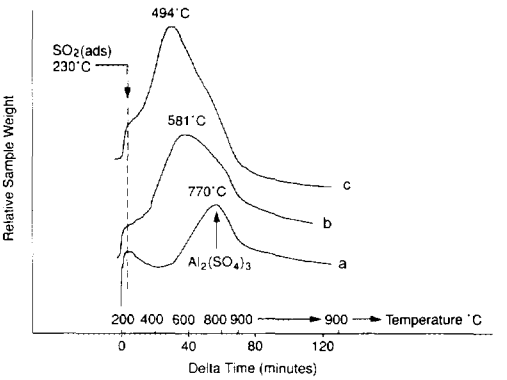

FIG. 7. Thermal gravimetric analyses of aluminum sulfate formation in catalyst samples. Reaction sequence:

$$SO_2(g) \rightarrow SO_2(ads) + O_2 \xrightarrow[\text{catalyst}]{}$$

$$SO_3(g) + Al_2O_3 \xrightarrow[\Delta]{} Al_2(SO_4)_3 \xrightarrow[\text{(surface)}]{} Al_2O_3 + SO_2(g).$$

Catalysts: (a) alumina blank, (b) 5% V_2O_5, and (c) 10% V_2O_5.

feature was clearly not related to the spectra of $AlVO_4$ in Fig. 4a. In fact, $AlVO_4$ was not detected in any of the samples. ^{51}V-MAS-NMR spectra of a physical mixture of the 5% Fe_2O_3 and 5% V_2O_5 samples after 900°C calcination were also obtained, but were essentially featureless.

Thermal Gravimetric Analysis— SO_2 Oxidation

Figure 7 shows typical TGA spectra for blank alumina (a), 5% V_2O_5 (b), and 10% V_2O_5 (c) catalysts. Common to all spectra was a low-temperature shoulder at about 230°C as well as a high-temperature peak ranging from 770°C for blank alumina (a), 581°C for the 5% V_2O_5 sample (b), and 494°C for the 10% V_2O_5 sample (c). The low-temperature shoulder is attributed to chemisorbed sulfur dioxide (*20*, *35*, *36*), whereas the high-temperature peak is due to the formation of aluminum sulfate on the surface, as demonstrated in similar earlier sulfur dioxide oxidation studies under isothermal conditions (*35*, *36*). The reaction sequence associated with Fig. 7 and derived from the results of earlier related studies (*35*) was as follows:

$$SO_2(gas) \xrightarrow{230\,^\circ C} SO_2(ads) + O_2 \xrightarrow[\text{Catalyst}]{} SO_3(g) + Al_2O_3 \xrightarrow[\Delta]{} Al_2(SO_4)_3 \xrightarrow[\Delta]{\text{(Surface)}} SO_2(g) + Al_2O_3.$$

The role of the catalyst (metal oxides) is to promote the oxidation of sulfur dioxide to the more reactive sulfur trioxide, which reacts with hydroxyl groups on the alumina surface to form aluminum sulfate. As aluminum sulfate forms, the sample gains weight. As the temperature increases further, aluminum sulfate decomposes to alumina plus gaseous sulfur dioxide and the sample loses weight.

The amount of aluminum sulfate formed on the catalyst surface was typically less than one monolayer for all samples. The maximum sample weight gain was similar

TABLE 8

TGA–SO_2 Oxidation Results[a]

Catalyst	Temperature at maximum sample weight gain (°C)	Initial sample color	Final residue color
PHF alumina	770	White	White
5% Fe_2O_3	590	Tan	Tan
5% V_2O_5	581	Yellow	Light green/yellow
10% Fe_2O_3	531	Tan	Yellow/tan
10% V_2O_5	494	Yellow	Yellow
5% V_2O_5–5% Fe_2O_3	507	Light green	Light green
5% V_2O_5 + 5%Fe_2O_3 (physical mixture)	584	Light green	Light green
10% $FeVO_4$ Std. + 90% PHF Al_2O_3	758	Light green	Light green
Silica (Cabosil EH-5)	No peak	White	White

[a] See Table 2 for oxidation program.

for all catalysts (about 3–4 wt%). Calculating a molecular diameter for adsorbed sulfur trioxide of about 0.1 m^2/μmole (following the method of Nam and Gavalas (*35*)), a 4-wt% gain in sample weight corresponds to about 25% coverage of the surface (190 m^2g) by sulfates.

The assignment of the high-temperature peak in Fig. 7 to aluminum sulfate formation/decomposition was further verified in a control experiment in which pure aluminum sulfate (Alfa, reagent) decomposed under the TGA test conditions over a 760–800°C temperature range. This temperature range brackets the reported thermal decomposition temperature of aluminum sulfate, 770°C, as reported in the CRC tables.

Table 8 lists the peak temperature and residue color of several catalysts subjected to the TGA-programmed SO_2 oxidation treatment described in Table 2. The initial and final colors of the samples in Table 8 were more or less the same, indicating negligible "gross" degradation of the sample during the TGA test. The uncertainty in the peak temperatures was about ±10°C. Total metals loading had the strongest impact on the peak temperatures in Table 8. The most active catalysts (i.e., those having the lowest peak temperatures) contained 10 wt% total metals in the order: 10% V_2O_5 (494°) > 5% Fe_2O_3–5% V_2O_5 (507°) > 10% Fe_2O_3 (531°C). Among the least active catalysts were alumina and a physical mixture of $FeVO_4$ standard (10 wt%) and alumina, with peak temperatures of 770 and 758°C, respectively. Blank silica (Cabosil EH-5, 300 m^2/g) was essentially inert.

Effect of Oxidizing Atmosphere on XRD Patterns

Table 9 shows the phase compositions of several samples either after air calcination at 900°C or after the TGA test, which also reached temperatures of 900°C in an SO_2/O_2 atmosphere (see Table 2). Table 9 shows that the type of oxidizing atmosphere had a significant effect both on the alumina phase formed as well as on the interactions of the metals in the samples. The 5% V_2O_5 sample formed θ-alumina and crystalline vanadium pentoxide after calcination in air at 900°C, whereas only γ-alumina was detected in the spent TGA residue. θ-Alumina and vanadium pentoxide were also detected on the spent 10% V_2O_5 sample, as seen in Table 9. In the 5% Fe_2O_3–5% V_2O_5 sample, a mixture of δ-alumina, κ-alumina, and vanadium pentoxide was formed after calcination at 900°C, whereas a mixture of γ- and δ-alumi-

TABLE 9

Effect of Oxidizing Atmosphere on the Catalyst XRD Phases

Catalyst	XRD phases after air calcination[a]		XRD phases after SO_2 TGA test[b]	
5% V_2O_5	θ-Al_2O_3 (Major) V_2O_5 (Minor)	Fig. 8b	γ-Al_2O_3 (Major)	Fig. 9b
10 % V_2O_5	—	—	θ-Al_2O_3 (Major) V_2O_5 (Minor)	—
5% Fe_2O_3	γ-Al_2O_3 (Major)	—	—	—
10% Fe_2O_3	—	—	γ-Al_2O_3 (Major)	—
5% V_2O_5–5% Fe_2O_3	δ-Al_2O_3 (Minor) K-Al_2O_3 (Major) V_2O_5 (Minor)	Fig. 8c	γ-Al_2O_3 (Intermediate) δ-Al_2O_3 (Intermediate) V_2O_5 (Minor)	Fig. 9c
PHF alumina blank	γ-Al_2O_3 (Major)	Fig. 8a	γ-Al_2O_3 (Major)	Fig. 9a

[a] After 900°C calcination—See Table 6.
[b] After TGA test—See Table 2.

nas, vanadium pentoxide, and a minor mixed iron–vanadium-oxide phase were detected in the spent TGA residue. For the blank PHF alumina sample and the iron sample, only the γ-alumina phase was present, regardless of oxidizing atmosphere, as shown in Table 9. Supporting XRD diffractograms for the assignments reported in Table 9 are shown as Figs. 8 and 9 for selected 900°C air-calcined samples of SO_2-TGA samples, respectively.

Figure 10 compares the baseline-corrected XRD patterns of the 5% Fe_2O_3–5% V_2O_5 catalysts after air calcination (a) and after TGA SO_2 oxidation treatment (b). The (a) and (b) patterns of Fig. 10 differ significantly due to the different alumina phases present in the two samples, as noted in Table 9.

A series of small peaks labelled "I" located between 25° and 30° two theta in pattern (b) of Fig. 10 may comprise an iron–vanadium mixed oxide labelled as $FeVO_x$ and most likely $FeVO_4$. While these peaks are relatively small in pattern (b), they were very prominent in commercially regenerated spent resid hydrotreating catalysts

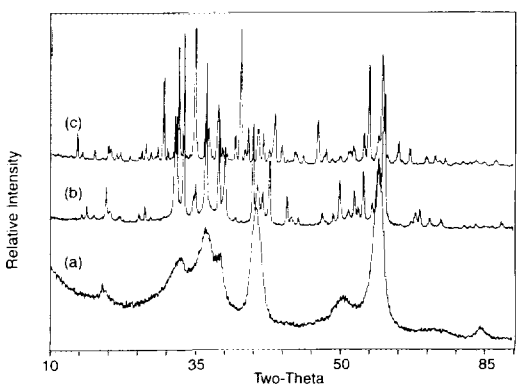

FIG. 8. Effect of 900°C air calcination on XRD patterns of catalysts: (a) blank alumina, (b) 5% V_2O_5, and (c) 5% Fe_2O_3–5% V_2O_5.

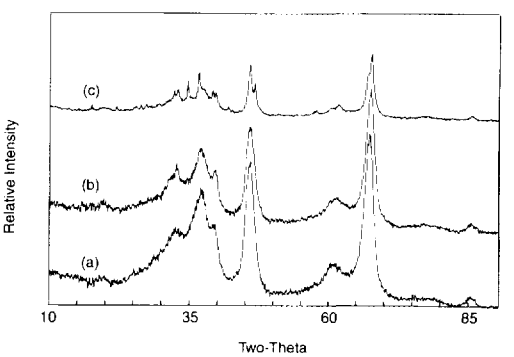

FIG. 9. Effect of TGA SO_2 oxidation test on XRD patterns of catalysts: (a) blank alumina, (b) 5% V_2O_5, and (c) 5% Fe_2O_3–5% V_2O_5.

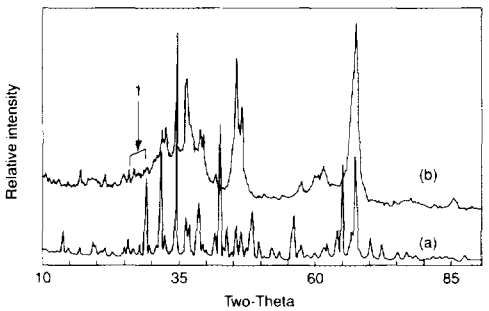

FIG. 10. Comparison of XRD patterns for 5% Fe_2O_3–5% V_2O_5 catalyst: (a) after 900°C calcination, (b) after TGA SO_2 oxidation, and (1) $FeVO_4$ mixed metal oxide.

(rich in iron and vanadium oxides) that had undergone extensive mesopore sintering and loss in attrition resistance following high-temperature decoking in the presence of sulfur dioxide (*22*).

Effect of Oxidizing Atmosphere on Alumina Crystallite Size

Table 10 shows differences in the sizes of alumina crystallites in selected samples subjected to different oxidizing atmospheres, i.e., either air calcination at 900°C or after the TGA test listed in Table 2. The results in Table 10 were calculated by applying the Scherrer equation to the 400 and 440 peaks (at 45.6° and 66.5° two theta) of the XRD patterns and averaging the results.

Table 10 shows that the alumina crystallite size of blank PHF alumina was the same, about 45–50 Å regardless of oxidizing atmosphere. However, the alumina crystallite size in the 5% V_2O_5 sample was 175 Å after air calcination at 900°C compared with only 55 Å after the TGA test. Finally, the crystallite size for the 5% V_2O_5–5% Fe_2O_3 sample after air calcination at 900°C was 270 Å compared with only 115 Å after the TGA test.

These results show that metal oxide–support interactions as well as the type of oxidizing atmosphere have significant effects on sintering of alumina crystallites in the samples. Air atmospheres seemed to cause more sintering of the alumina crystallites than did the SO_2/O_2 atmosphere of the TGA test.

DISCUSSION

Intraparticle Vanadium Migration (SPS)

The results of Table 4 suggest that extensive vanadium migration to the particle surface occurs at high calcination temperatures and that the vanadium migration is enhanced when iron is present. Moreover, the bulk analyses of Table 3 show that vanadium is not being volatilized from the catalysts under the calcination conditions employed. Concentrations of iron in the 5% Fe_2O_3 catalyst and the 5% V_2O_5–5% Fe_2O_3 catalyst remain relatively constant both on the surface (Table 4) and in the bulk (Table 3) over this same range of calcination temperatures.

Though vanadium migration is known to occur under conditions similar to those in our study, (*2–8*) intraparticle vanadium migration that is enhanced by iron has not been observed before. The relatively constant Fe/Al ratio suggests that iron either remains fixed on the catalyst surface at temperatures from 500 to 900°C, or that iron is absorbed into the alumina lattice as low as 500°C. Mössbauer results below suggest that both may occur.

Origin of −200 ppm Feature in ^{51}V-NMR Spectra

The origin of the −200-ppm spectral feature in the 5% V_2O_5 sample calcined at 900°C (Fig. 5c) is not well understood, however,

TABLE 10

Effect of Oxidizing Atmosphere on Alumina Crystallite Size (Å)

Catalyst	After 900°C air calcination	After TGA test (Table 2)
PHF alumina blank	45	50
5% V_2O_5	175	55
5% V_2O_5–5% Fe_2O_3	270	115

sodium contamination (e.g., formation of sodium vanadate) and instrument artifacts have been ruled out. Two distinct surface vanadate species are known to exist on alumina supports with similar surface coverages of vanadium oxide—octahedrally coordinated decavanadates and monomeric tetrahedrally coordinated metavanadates—based on both Raman and static NMR measurements (*34*). The −200-ppm feature is hypothesized to be one of these two surface vanadates, whereas the 0-ppm feature is due to crystalline vanadium pentoxide.

Interestingly, the absence of the −200-ppm feature in the 5% V_2O_5–5% Fe_2O_3 sample calcined at 900°C (Fig. 6c) may be due to signal dampening by the close proximity of the surface vanadate species above to the ferromagnetic iron in the sample. However, the size of the vanadium pentoxide crystallites in the coimpregnated iron–vanadium sample may apparently be large enough (at least 50 Å (*37*)) as not to be dampened by the iron.

Interparticle Vanadium Migration (NMR)

The featureless ^{51}V-NMR spectra exhibited by the physical mixture of 5% V_2O_5 and 5% Fe_2O_3 after 900°C calcination may indicate that vanadium has migrated from the 5% V_2O_5 particles to the 5% Fe_2O_3 particles, where the close proximity of the vanadium to the paramagnetic surface iron would damp out the vanadium NMR signal. Moreover, the net surface coverage of vanadium on the 5% V_2O_5 particles after this migration occurred apparently may have been less than one monolayer and, thus, insufficient to form a bulk crystalline vanadium pentoxide phase (*9*). Vanadium does not volatilize from the catalyst under these conditions, as indicated in Table 3.

The results of the physical mixture experiment indicate that interparticle migration of the vanadium may occur at 900°C under our conditions. We cannot quantify the extent of the migration. Interparticle vanadium migration was first demonstrated by Occelli (*45*). The work was later duplicated by Altomare *et al.* (*5*), who demonstrated interparticle vanadium migration using physical mixtures of vanadium-doped silica–alumina microspheres and conventional zeolite-containing microspheres. Their steaming experiments at about 800°C confirmed that about 80% of the vanadium on the vanadium-doped particles had migrated to the vanadium-free particles (*5*).

Iron Interactions (Mössbauer)

All spectra shown in Fig. 2 and 3 contain a superparamagnetic doublet, which has been assigned to Fe(+3) ions absorbed into the alumina lattice (*14–19*). However, the calcination temperature at which this solid solution formed has varied in the literature, ranging from 400 (*16*) to 1050°C (*17*). Moreover, one study showed that both a solid solution and a well-dispersed surface Fe_2O_3 particle of less than 100 Å size was formed if at least 1 wt% Fe was impregnated on γ-alumina and then calcined at 600°C (*15*).

The quadrupole splitting is inversely proportional to the iron particle size and proportional to the degree of iron dispersion (*14*, *26*, *27*). XRD analyses failed to detect crystalline Fe_2O_3 phases (with a limit of detection of 50 Å crystallite size) in the samples. Moreover, separate Raman studies (*43*) did not detect any crystalline Fe_2O_3 phases in the samples, except for the 5% Fe_2O_3 samples (which contained only traces of α-Fe_2O_3). Thus, the sharp decrease in the quadropole splitting for the 5% V_2O_5–5% Fe_2O_3 sample with increase in calcination temperature (Table 7) may possibly indicate a decrease in iron dispersion, or perhaps an increase in the Fe–Fe interaction caused by the loss in surface area.

Mössbauer spectra of samples subjected to subambient temperatures is another method used to detect crystalline Fe_2O_3 phases in a sample, since the size of an Fe_2O_3 particle is proportional to the temperature at which the conversion from superparamagnetic to ferromagnetic behavior occurs (*14*, *27*).

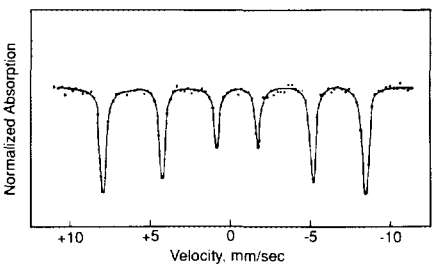

FIG. 11. Mössbauer spectra of reference ferromagnetic α-Fe_2O_3 showing hyperfine Zeeman splitting (*25*).

Ferromagnetism results in the 6-line Zeeman pattern shown in Fig. 11 for reference bulk α-Fe_2O_3. The lack of magnetic hyperfine splitting at temperatures as low as 4.2 K for the 5% Fe_2O_3–V_2O_5 catalyst in Fig. 2c and as low as 1.4 K for the 5% Fe_2O_3 catalyst in Fig. 3d suggests that the iron may be substituted for aluminum in the alumina lattice. However, surface crystalline α-Fe_2O_3 species could also exist (*15*). XPS or ESCA analysis of the samples in a severely reduced state would be useful for quantifying the surface iron, which reduces to metallic Fe, and the absorbed iron, which reduces to Fe(+2) (*15*, *28*). These experiments were not performed. However, Raman studies of these same samples showed that the iron was generally well dispersed, with only traces of crystalline α-Fe_2O_3 found in the 5% Fe_2O_3 sample after calcination temperatures ranging from 500 to 900°C (*43*).

TGA Results

Since sulfate coverage on the samples was similar and never exceeded a quarter monolayer during the TGA test (as confirmed by the absence of aluminum sulfate by postmortem XRD in Table 9), the high-temperature peak in Fig. 7 was the pertinent measurement in the TGA experiment. This peak gave an indication of the intrinsic catalyst activity for oxidizing SO_2 from which metal oxide–metal oxide interactions might be inferred.

Our TGA test results confirm that iron oxide and vanadium pentoxide had high activities for oxidizing sulfur dioxide to the trioxide (*20*, *36*). Moreover, the fact that the 5% Fe_2O_3–5% V_2O_5 sample had high activity whereas the $FeVO_4$/alumina sample had low activity (similar to the alumina blank) suggests that:

1. Surface V_2O_5 and Fe_2O_3 phases accelerate SO_2 oxidation.
2. Mixed-metal $FeVO_4$ oxide is inactive for SO_2 oxidation.
3. Iron and vanadium oxides do not form significant amounts of $FeVO_4$ or related mixed oxides in the 5% Fe_2O_3–5% V_2O_5 sample.

Metal Oxide–Support Interactions

Figures 12 and 13 exemplify a variety of metal oxide–support interactions that occur as a function both of dispersed metal oxide type as well as the oxidizing atmosphere. In the samples subjected to air calcination, a variety of alumina phases were observed. In the 5% V_2O_5 catalyst, the predominant phase was θ-alumina (Fig. 12a), as suggested by XRD results in Fig. 8b. In the 5% Fe_2O_3 sample (Fig. 12b), Mössbauer results in Fig. 3 suggested that iron may be present in the form of small (<50 Å) α-Fe_2O_3 surface oxides or that Fe(+3) ions may be absorbed into the alumina lattice, or both. Also, Raman analyses confirmed the existence of traces of α-Fe_2O_3 crystallites (*43*) (Figure 10b). In the 5% Fe_2O_3–5% V_2O_5 catalyst, a mixture of δ- and κ-aluminas was formed after high-temperature air calcination (Fig. 12c), as suggested by XRD results in Fig. 8c.

On the other hand, in the samples subjected to the TGA treatment, a surprisingly greater retention of the γ-alumina phase was observed. The 5% V_2O_5 catalyst, the 5% Fe_2O_3 catalyst, and the 5% Fe_2O_5–5% V_2O_5 catalyst (Figs. 13a, 13b, and 13c, respectively) all contained predominantly γ-alumina as well as a surface phase of aluminum sulfate (less than monolayer coverage). In Fig. 13c, the 5% Fe_2O_3–5% V_2O_5 catalyst

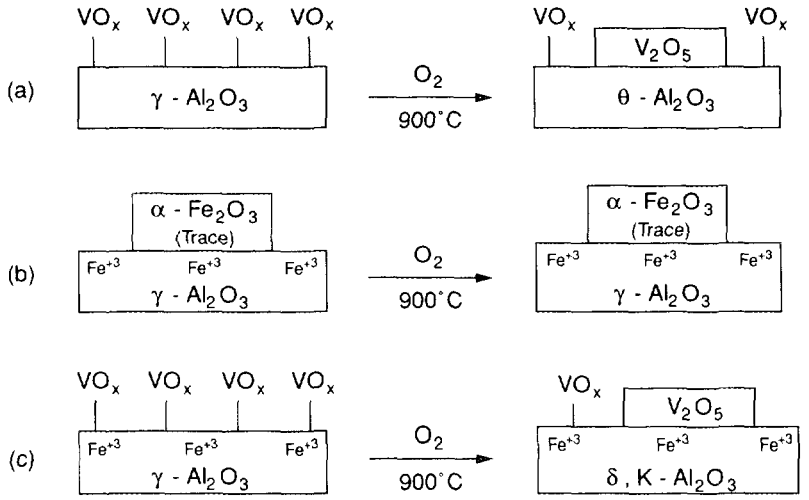

FIG. 12. Effect of calcination on iron and vanadium catalysts: (a) 5% V_2O_5, (b) 5% Fe_2O_3, and (c) 5% V_2O_5–5% Fe_2O_3.

had a mixture of both γ-alumina and δ-alumina. XRD analyses in Table 9 and Figs. 8–10 formed the basis for most of these assignments.

Metal Oxide–Metal Oxide Interactions

Figures 12c and 13c exemplify differences in metal oxide–metal oxide interactions in the 5% Fe_2O_3–5% V_2O_5 samples as a function of oxidizing atmosphere. As seen in Fig. 13c, minor crystalline phases of vanadium pentoxide and an iron–vanadium-mixed oxide labelled as $FeVO_x$ were detected, based on the results in Fig. 10 and Table 9. However, $FeVO_x$ formation was not observed following calcination in air at 900°C (Fig.

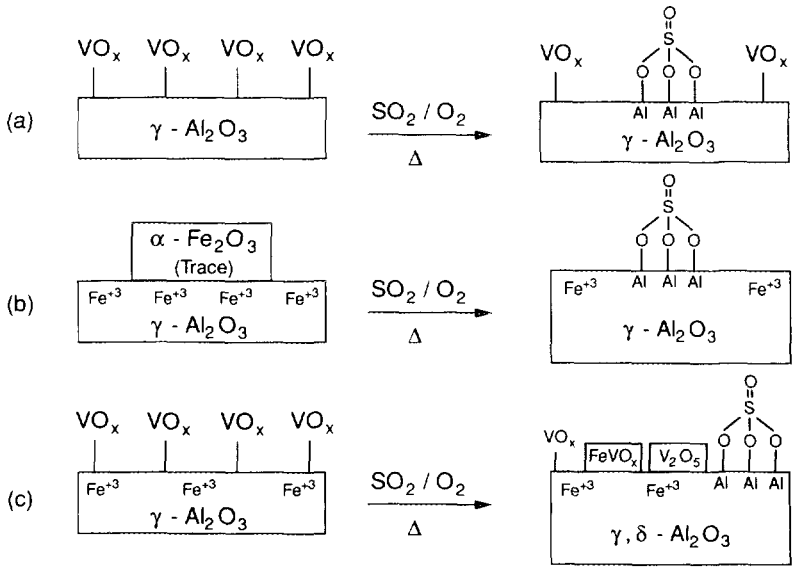

FIG. 13. Effect of TGA SO_2 oxidation test on iron and vanadium catalysts: (a) 5% V_2O_5, (b) 5% Fe_2O_3, and (c) 5% V_2O_5–5% Fe_2O_3.

12c) based on the XRD results in Table 9. The formation of $FeVO_4$ in the TGA sample residue may result from surface iron oxide "precipitating out of solution" due to the formation of the aluminum sulfate overlayer on the catalyst surface. This "precipitated" iron oxide may then react with the migrating vanadium to form the $FeVO_4$ species detected by XRD in Fig. 10b. While such a mechanism is only hypothesized, it is interesting to note that no $FeVO_4$ species is observed in any air calcined sample.

Alumina Pore Sintering Model

Metal oxide additives, pretreatment atmospheres and even particle morphology can accelerate or decelerate the rate of surface-area loss and phase transformations in alumina catalysts (*13*, *38*). An alumina pore sintering model proposed by Johnson suggests that phase transformations in alumina proceed by a mechanism involving the condensation of hydroxyl groups between adjacent alumina crystallites, forming Al–O–Al linkages at high temperature (*38*). Stabilizing metals slow this phase transformation by replacing or capping off hydroxyl groups on the alumina surface, thus reducing the rate of Al–O–Al formation (*38*). In our study, XPS, NMR, XRD, and porosimetry all showed that vanadium pentoxide may catalyze the dehydroxylation of surface hydroxyl groups and destabilize the catalyst pore structure and phase composition, especially at higher temperatures. This phenomenon has also been observed by others (*9*, *39–41*).

However, when a catalyst containing vanadium pentoxide was exposed to sulfur dioxide under the conditions of our TGA test, the alumina retained significantly more of the γ-phase, as seen by comparing the results in Table 9. The model of Johnson appears to account for these observations since surface overlayers of aluminum sulfate may stabilize the alumina by retarding the rate of condensation between adjacent hydroxyl groups.

The enhanced rate of surface area loss for the 5% Fe_2O_3–5% V_2O_5 catalyst, compared with the 5% V_2O_5 catalyst in Table 5, may be a consequence of two different surface vanadate species in the two respective catalysts. Complementary Raman studies showed that vanadium existed primarily as a metavanadate monomer species (VO_4^{-2}) in the 5% V_2O_5 samples compared with a pyrovanadate dimer species ($V_2O_7^{-4}$) in the 5% Fe_2O_3–5% V_2O_5 samples over the 500–800°C temperature range (*43*). Although the diffusivities of these two vanadate species on the catalyst surface have not been measured, the higher rate of surface-area loss for the 5% Fe_2O_3–5% V_2O_5 sample may indicate more rapid diffusion of the pyrovanadate compared with the metavanadate species and thus enhanced rates of dehydroxylation of the alumina surface under our oxidation conditions.

Impact of Sulfur Dioxide in Laboratory Aging of FCC Catalysts

The results of this study suggest a possible need to incorporate a sulfur dioxide treatment step during typical laboratory aging of fresh FCC catalyst, especially if contaminant metals have been artificially introduced. Sulfur dioxide reacts to form an aluminum sulfate overlayer on the catalyst surface, which results in different metal oxide–metal oxide interactions and alumina phase changes compared with calcinations free of sulfur dioxide. The interactions impact directly on alumina (phase stabilization) and indirectly on the supported metals, iron and vanadium.

Typically, FCC catalysts are laboratory aged by doping with vanadium precursors and/or by steaming at high temperatures to equilibrate the catalyst under simulated FCC regeneration conditions (*3–8*). The most commonly used FCC aging procedure was defined by Mitchell (*46*). This has generally been the accepted industry practice. However, steam alone may not be sufficient to simulate actual conditions in an FCC regenerator. As our study shows, sulfur dioxide, a combustion by-product, can influence

the catalyst surface chemistry and phase transformations. Steam itself simply accelerates the formation of phases that are already thermodynamically stable at the given temperature (*3*, *13*, *38*).

In the literature, only two references could be found which dealt with the impact of sulfur dioxide on metal oxide–metal oxide or metal oxide–support interactions under typical FCC regeneration conditions. The first introduces a new vanadium trap called CVP-4 and emphasizes the "impact of sulfur" in testing the true passivating potential of this and similar materials (*42*). (CVP-4 is a physical mixture of dolomite (calcium–magnesium oxide) and sepiolite (magnesium silicate) particles (*42*)). The second deals with vanadium migration and the thermodynamics of sulfate poisoning of passivating agents in FCC regeneration (*3*).

Laboratory catalyst aging procedures employing artificial metals loading followed by steam deactivation should be reexamined to assess the need for a possible sulfur dioxide treatment step. The results of this study show that significant changes occur in alumina-based samples that may well occur to a similar extent in sieve-based FCC catalysts, which also contain alumina.

CONCLUSIONS

1. Wide variations in surface-area stability, phase composition, metal oxide–metal oxide interactions, and interparticle metal oxide migration were observed in PHF γ-alumina samples containing iron and/or vanadium oxides that were subjected to oxidizing conditions chosen to simulate FCC or resid catalyst regeneration conditions. Samples were subjected to calcination temperatures from 500 to 900°C and were also tested for the oxidation of sulfur dioxide by thermal gravimetric analysis (TGA).

2. In the calcined samples, vanadium migrated to the catalyst particle surface at elevated temperatures, forming crystalline phases of vanadium pentoxide and θ-alumina. This effect was enhanced in the presence of iron, with additional phases of alumina formed.

3. TGA tests indicated that both iron and vanadium oxides catalyzed the formation of sulfur trioxide from sulfur dioxide and thus promoted the formation of aluminum sulfate at lower temperatures compared with blank alumina. Iron–vanadium mixed metal oxides were apparently inactive. Vanadium-containing samples subjected to the sulfur dioxide TGA test retain the γ-alumina phase, unlike samples subjected to air calcination, which formed other low-surface-area alumina phases. Interestingly, XRD evidence suggested that iron–vanadium mixed oxides may form during the TGA test, whereas no such interaction was observed during air calcination.

4. The results were interpreted in terms of an existing model for hydrothermal sintering of aluminas.

5. The results of this study suggest a possible need to incorporate a sulfur dioxide treatment step during typical laboratory aging of fresh FCC catalyst, especially if contaminant metals have been artificially introduced. Sulfur dioxide reacts to form an aluminum sulfate overlayer on the catalyst surface, which results in different metal oxide–metal oxide interactions and alumina phase changes compared with calcinations free of sulfur dioxide. The impact of sulfur dioxide in FCC steaming procedures should be assessed.

ACKNOWLEDGMENTS

Many people made significant contributions to this work. Discussions with Naresh Sethi (V-NMR), Bob Roginski (Raman), Bernie Meyers and Bob Whittaker (TGA), Jim Kaduk, Maria Kaminsky, and Ying-Mei Chen (XRD), and Joe Shyu (XPS), all of Amoco Corporation, were invaluable to the interpretation. Dr. William Reiff of Mössbauer Spectroscopy Consultants in Bethlehem, Massachusetts, obtained the Mössbauer spectra and is acknowledged for several helpful discussions. Professor W. N. Delgass (Purdue University) also provided additional insights that were helpful to the interpretation. Technical assistance at Amoco was provided by Bob Whittaker (TGA, porosimetry), Ying-Mei Chen and Maria Kaminsky (XRD), Claude Price (NMR), Than Nguyen (XPS) and Jutta Schreiner (XPS), Harold Marcoux (Raman), and Isobel Harpower (ICP).

REFERENCES

1. Trimm, D. L., *in* "Catalysts in Petroleum Refining 1989" (D. L. Trimm *et al.*, Eds.), p. 41, Elsevier, Amsterdam, 1990.
2. Biswas, J., and Maxwell, I. E., *Appl. Catal.* **63,** 197 (1990).
3. Wormsbecher, R. F., Peters, A. W., and Maselli, J. M., *J. Catal.* **100,** 130 (1986).
4. Pine, L. A., *J. Catal.* **125,** 514 (1990).
5. Altomare, C. A., Koermer, G. S., Martins, E., Schubert, P. F., Suib, S. L., and Willis, W. S., *Appl. Catal.* **45,** 291 (1988).
6. Jones, R. L., *J. Catal.* **129,** 269 (1991).
7. Anderson, M. W., Occelli, M. L., and Suib, S. L., *J. Mol. Catalysis,* **61,** 295 (1990).
8. Occelli, M. L., Psaras, D., and Suib, S. L., *J. Catal.* **96,** 363 (1985).
9. Wachs, I. E., Jehng, J. M., and Hardcastle, F. D., *Solid State Ionics* **32/33,** 904 (1989).
10. Wachs, I. E., *Chem. Eng. Sci.* **45,** 2561 (1990).
11. "New Directions in Catalysis By Oxides," Catalytica Study No. 4190 CO, Catalytica, Mountain View, CA, 1990.
12. Hopkins, P. D., Meyers, B. L., *Ind. Eng. Chem. Prod. Res. Dev.* **22,** 421 (1983).
13. Trimm, D. L., *in* "Studies in Surface Science and Catalysis" (J. B. Butt and C. H. Bartholomew, Eds.), Vol. 68, p. 38, Elsevier, Amsterdam, 1991.
14. Gager, H. M., and Hobson, M. C., *Catal. Rev. Sci. Eng.* **11,** 117 (1975).
15. Hoffman, D. P., Ph.D. thesis, University of Pittsburgh, 1989.
16. Strohmeier, B. R., Ph.D. thesis, University of Pittsburgh, 1984.
17. Bhide, V. G., and Date, S. K., *Phys. Rev.* **172**(2), 345 (1968).
18. Hobson, M. C., and Gager, H. M., *J. Catal.* **16,** 254 (1970).
19. Korecz, L., Kurucz, I., Menczel, G., Papp-Molnar, E., Pungor, E. and Burger, K., *Talanta* **19,** 1599 (1972).
20. Hirschberg, E. H., and Bertolacini, R. J., *in* "Fluid Catalytic Cracking: Role in Modern Refining" (M. L. Occelli, Ed.), pp. 115–145, ACS Symposium Series 375, Amer. Chem. Soc., Washington, DC, 1988.
21. Lowell, P. S., Schwitzgebel, K., Parsons, T. B., and Sladek, K. J., *Ind. Eng. Chem. Process Des. Dev.* **10,** 384 (1971).
22. Clark, F. T., Hensley, A. L., Shyu, J. Z., Kaduk, J. A., and Ray, G. J., *in* "Studies in Surface Science and Catalysis" (J. B. Butt and C. H. Bartholomew, Eds.), Vol. 68, p. 419, Elsevier, Amsterdam, 1991.
23. Wong-Ng, McMurdie, W., *et al.*, National Bureau of Standards, JCPDS Grant in Aid Report, JCPDS-ICPD 38-1372, 1987.
24. Bankcroft, G. M., Maddock, A. G., Ong, W. K., Prince, R. H., and Stone, A. J., *J. Chem. Soc. America* **1966** (1967).
25. Greenwood, N. N., and Gibb, T. C., "Mössbauer Spectroscopy," pp. 240–247, Chapman and Hall, London, 1971.
26. Drago, R. S., "Physical Methods in Chemistry," p. 541, W. B. Saunders, Philadelphia, 1977.
27. Anderson, J. R., and Pratt, K. C., "Introduction to Characterization and Testing of Catalysts," p. 387, Academic Press, Orlando, 1985.
28. Delgass, W. N., Purdue University, personal communication.
29. Deo, G., Hardcastle, F. D., Richards, M., Hirt, A. M., and Wachs, I. E., *in* "Novel Materials in Heterogeneous Catalysis" (R. T. Baker, L. L. Murrell, Eds.), Chap. 29, p. 321, American Chemical Society, 1990.
30. Bergeret, G., Gallezot, P., Chary, K. V. R., Rao, B. R., and Subrahmanyam, V. S., *Appl. Catal.* **40,** 191 (1988).
31. Inomata, M. J., Morl, K., Miyamoto, A., and Murakami, Y., *J. Phys. Chem.* **87,** 761 (1983).
32. Roozeboom, F., Mitteimeijer-Hazeleger, M. C., Moulijn, J. A., Mederna, J., and deBeer, V. H. J., *J. Phys. Chem.* **84,** 2783 (1986).
33. Eckert, H., and Wachs, I. E., *Mater. Res. Soc. Symp. Proc.* **111,** 459 (1988).
34. Eckert, H., and Wachs, I. E., *J. Phys. Chem.* **93,** 1017 (1989).
35. Nam, S. W., and Gavalas, G. R., *Appl. Catal.* **55,** 193 (1989).
36. Nam, S. W., and Gavalas, G. R., *Appl. Catal.* **75,** 53 (1991).
37. Sethi, N. K., Amoco Corporation Research and Development, private communication.
38. Johnson, M. L., *J. Catal.* **123,** 245 (1990).
39. DelArco, M., Holgado, M. J., Martin, C., and Rives, V., *Langmuir* **6,** 801 (1990).
40. Sobalik, Z., Kozlowski, R., and Haber, J., *J. Catal.* **127,** 665 (1991).
41. Bond, G. C., and Konig, P., *J. Catal.* **77,** 309 (1982).
42. Jossens, L. W., and Kennedy, J. V., *Prepr. Am. Chem. Soc. Div. Pet. Chem.* **35**(4), 768, 1990; associated patents: US 4,988,654 and US 5,002,653.
43. Wachs, I. E., Jehng, J. M., Clark, F. T., and Springman, M. C., submitted for publication.
44. Barrett, E. P., Joyner, L. G., Halenda, P. T., *J. Am. Chem. Soc.* **73,** 373 (1951).
45. Occelli, M. L., *ACS Symp. Ser.* **375,** 162 (1987).
46. Mitchell, B. R., *Ind. Eng. Chem. Prod. Res. Dev.* **19,** 209 (1980).
47. Robertson, B., Kostiner, E., *J. Solid State Chem.* **4,** 29, (1972).